Linear and nonlinear photonic Jackiw-Rebbi states in interfaced binary waveguide arrays

Truong X. Tran[1] and Fabio Biancalana[2]
[1]*Department of Physics, Le Quy Don University, 236 Hoang Quoc Viet Street, 10000 Hanoi, Vietnam*
[2]*School of Engineering and Physical Sciences, Heriot-Watt University, EH14 4AS Edinburgh, United Kingdom*
(Received 22 February 2017; published 17 July 2017)

We study analytically and numerically the optical analog of the Jackiw-Rebbi states in quantum-field theory. These solutions exist at the interface of two binary waveguide arrays, which are described by two Dirac equations with masses of opposite sign. We show that these special states are topologically robust not only in the linear regime, but also in the nonlinear one (with both focusing and defocusing nonlinearities). We also reveal that one can effectively generate Jackiw-Rebbi states starting from Dirac solitons.

DOI: 10.1103/PhysRevA.96.013831

I. INTRODUCTION

Waveguide arrays (WAs) present a unique discrete periodic system to investigate many interesting photonic phenomena such as discrete diffraction [1,2] and discrete solitons [1,3]. At the interface between two different semi-infinite one-dimensional (1D) WAs, surface solitons can occur [4–6]. The surface solitons can also exist at the interface between a uniform medium and a WA and have been investigated both theoretically [7–9] and experimentally [10–12].

Waveguide arrays have also been used intensively to simulate the evolution of a nonrelativistic quantum mechanical particle in a periodic potential [13]. Many fundamental phenomena in nonrelativistic classical and quantum mechanics such as Bloch oscillations [14,15] and Zener tunneling [16,17] have been investigated both theoretically and experimentally by using WAs. It was shown in recent studies that most of the nonlinear phenomena usually associated with fiber optics (such as the emission of resonant radiation from solitons and soliton self-frequency shift) can also take place in specially excited WAs, but in the spatial domain rather than in the temporal domain [18,19]. In addition, a supercontinuum in both frequency and wave number domains can be generated in nonlinear WAs [20]. Binary waveguide arrays (BWAs) have been used to mimic relativistic phenomena typical of quantum field theory (QFT), such as Klein tunneling [21,22], Zitterbewegung (trembling motion of a free Dirac electron) [23,24], and fermion pair production [25], which are all based on the properties of the Dirac equation [26]. The discrete gap solitons in BWAs in the *classical* context have been investigated both numerically [27,28] and experimentally [29]. Gap and out-gap solitons and breathers in BWAs have been investigated as well [30,31]. These gap solitons were already known in [32] for diatomic lattices and later derived in their continuum-limit form for the BWA system in [30]. Recently, the explicit suggestion to use BWAs to simulate a quantum nonlinear Dirac equation was put forward in [33], where the gap solitons in BWAs were shown to be connected to Dirac solitons (DSs) in a nonlinear extension of the relativistic 1D Dirac equation describing the dynamics of a freely moving relativistic particle. The 1D DS stability, its dynamics, and different scenarios of soliton interaction were systematically investigated in [34]. The formation and dynamics of two-dimensional DSs in square binary waveguide lattices also were considered in [35]. The higher-order Dirac solitons in BWAs were studied in [36]. Although there is currently no evidence for fundamental quantum nonlinearities, nonlinear versions of the Dirac equation have been studied for a long time, mainly because they allow the exploration of extreme physical environments, such as Dirac particles dynamics in astrophysical objects [37], or the influence of fermion fields in general relativity singularities [38]. One of the earlier extensions was investigated by Heisenberg himself [39] in the context of field theory and was motivated by the question of mass. In the quantum mechanical context, nonlinear Dirac equations have been used as effective theories in atomic, nuclear, and gravitational physics [40–43]. In this regard, BWAs can offer a unique platform to simulate nonlinear extensions of the Dirac equation when probed at high light intensities.

Topological photonics is an important emerging field that allows the control and manipulation of light propagation by using regions of space with different topological numbers (such as the Chern number or the winding number), where light is forced to follow predetermined paths. For instance, this concept has allowed the fabrication of gyromagnetic ferrite photonic crystals, where an external magnetic field induced states with nonvanishing Chern numbers [44]. Topological photonics also promises to provide robust transport of optical modes by suppressing backscattering [44,45]. Therefore, conceptually, topological photonics can potentially play a crucial role in the development of robust and practical optical circuits for the unidirectional transport of light [44].

Another peculiar result emerging from the Dirac equation is that one can observe the existence of a special topological state, known in QFT as a Jackiw-Rebbi (JR) solution [46]. Originally, the JR model was introduced in order to couple a fermion with a scalar field, the latter being a solution of the ϕ^4 model, i.e., a solitonic kink in $1+1$ dimensions [46]. This coupling allowed the smooth variation of the Dirac particle mass from negative to positive, whereas a new topological state could carry a half-integer fermion number [46].

The JR state is well known for predicting the charge fractionalization phenomenon, which is fundamental to the fractional quantum Hall effect [47]. The JR state is also well known for the topological nature of its zero-energy solution and can be interpreted as a precursor to topological insulators, which have attracted much interest recently [48,49]. The photonic topological defect states on the edge of a BWA were experimentally observed in [50]. Quite recently, the

 ©2017 American Physical Society

topological defect mode at the interface between two periodic dimer chains was also demonstrated [51]. So far, several schemes have been proposed to realize the JR state and observe charge fractionalization such as by using an atomic Fermi-Dirac gas loaded in a periodic optical lattice [52] or by using so-called heavy solitons in a fermionic superfluid [53]. Recently, a photonic implementation of the JR model in a slow-light polaritonic setup was also proposed [54].

In this work we explore another possibility of creating the optical analog of the JR solution. This solution is a type of topological edge state, which exists at the (continuous or discontinuous) interface of two binary waveguide array regions where the Dirac mass parameter changes sign. We study the linear and *nonlinear* properties of the JR state, which is possible by using the Kerr nonlinearity of the waveguides forming the array. Finally, we explore the excitability of JR states starting from two Dirac solitons with masses of opposite sign, propagating individually in each waveguide array. This new photonic state can have important applications in light manipulation and circuitry or in the generation of robust, topologically protected correlated photon sources.

II. GOVERNING EQUATIONS

Light propagation in a discrete, periodic binary array of Kerr nonlinear waveguides can be described, in the monochromatic regime, by the dimensionless coupled-mode equations [21]

$$i\frac{da_n(z)}{dz}+\kappa[a_{n+1}(z)+a_{n-1}(z)]-(-1)^n\sigma a_n + \gamma|a_n(z)|^2a_n(z)=0, \tag{1}$$

where a_n is the electric-field amplitude in the nth waveguide, z is the longitudinal spatial coordinate, 2σ and κ are the propagation mismatch and the coupling coefficient between two adjacent waveguides of the array, respectively, and γ is the nonlinear coefficient of waveguides, which is positive for self-focusing, but negative for self-defocusing media. For $n<0$ (for the left-hand-side BWA), $\sigma=\sigma_1$, whereas for $n\geqslant 0$ (the right-hand-side BWA), $\sigma=\sigma_2$.

After setting $\Psi_1(n)=(-1)^n a_{2n}$ and $\Psi_2(n)=i(-1)^n a_{2n-1}$ and following the standard approach developed in [23,24] we can introduce the continuous transverse coordinate $\xi\leftrightarrow n$ and the two-component spinor $\Psi(\xi,z)=(\Psi_1,\Psi_2)^T$, which satisfies the 1D nonlinear Dirac equation [33]

$$i\partial_z\Psi=-i\kappa\hat{\sigma}_x\partial_\xi\Psi+\sigma\hat{\sigma}_z\Psi-\gamma G, \tag{2}$$

where the nonlinear terms $G\equiv(|\Psi_1|^2\Psi_1,|\Psi_2|^2\Psi_2)^T$ and $\hat{\sigma}_x$ and $\hat{\sigma}_z$ are the usual Pauli matrices. In QFT the parameter σ in the Dirac equation is often called the mass of the Dirac field (or Dirac mass) and this mass parameter can be both positive and negative (see, for instance, Ref. [55] for more details).

III. LOCALIZED JACKIW-REBBI STATES IN THE LINEAR CASE

If $\sigma_1<0$ and $\sigma_2>0$ we get the following exact localized solution of Eq. (2) in the linear case:

$$\Psi(\xi)=\sqrt{\frac{|\sigma_1\sigma_2|}{\kappa(|\sigma_1|+|\sigma_2|)}}\begin{pmatrix}1\\ i\end{pmatrix}e^{-|\sigma(\xi)\xi|/\kappa}. \tag{3}$$

Specifically, when the Dirac mass term $\sigma(\xi)$ has the form of the hyperbolic tangent function one can find localized JR states for the Dirac equations, which are often called the zero-mode zero-energy states [see Eqs. (2.4)–(2.6) in [46], Eq. (1) and Fig. 1(a) in [53], and also Eqs. (1)–(4) and Fig. 1 in [54]]. Note that, in our case, the Dirac mass term $\sigma(\xi)$ has the form of a steplike function, which leads to the localized solution in the form of Eq. (3), and it thus corresponds to the limit when the scale kink of the JR model has an infinite steepness. What is important here is the difference in sign of the Dirac mass in adjacent BWAs and not the smoothness of the transition. The solution (3) is the exact one to Eq. (2), but it is an approximate solution to the discrete equation (1). Obviously, this approximation will become better if the beam width gets larger. If $|\sigma_1|=|\sigma_2|=\sigma_0$, one can easily get the following exact localized solutions for the discrete equation (1) without nonlinearity ($\gamma=0$) for the following two cases. (i) If $-\sigma_1=\sigma_2=\sigma_0>0$, one gets the following JR state of the 1st type

$$a_n=b_n e^{i[\kappa-\sqrt{\sigma_0^2+\kappa^2}]z}, \tag{4}$$

where b_n is real and independent of the variable z, $b_{2n-1}=b_{2n}$. For $n\geqslant 0$ (the right-hand side BWA) one has the relationship $b_{2n}/b_{2n+1}=\alpha\equiv-[\sigma_0/\kappa+\sqrt{1+\sigma_0^2/\kappa^2}]$, whereas for $n<0$ (the left-hand side BWA) one has $b_{2n+1}/b_{2n}=\alpha$. (ii) However, if $\sigma_1=-\sigma_2=\sigma_0>0$, one has the following JR state of the 2nd type

$$a_n=b_n e^{i[\kappa+\sqrt{\sigma_0^2+\kappa^2}]z}, \tag{5}$$

where b_n is again real and independent of the variable z, $b_{2n-1}=b_{2n}$. For $n\geqslant 0$ one has $b_{2n}/b_{2n+1}=-\alpha$, whereas for $n<0$ one has $b_{2n+1}/b_{2n}=-\alpha$.

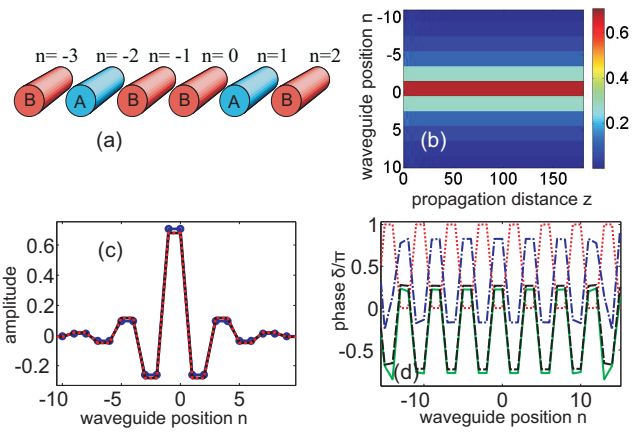

FIG. 1. (a) Illustrative sketch of two BWAs with opposite propagation mismatches located adjacent to each other. (b) Propagation of a beam in the linear regime where Eq. (3) is used as the input condition. (c) Curves showing the amplitudes of the beam at the input (solid blue with round markers) and output (solid black), which are hidden behind the dotted red curve representing the solution in the form of Eq. (4). (d) Phase pattern of the beam in (a) at different propagation distances $z=0$ (dotted red), 100 (dash-dotted blue), 150 (solid green), and 200 (dashed black). The parameters are $-\sigma_1=\sigma_2=1$, $\kappa=1$, and $\gamma=0$. Two BWAs consist of 841 waveguides in total.

In Fig. 1(a) we show the illustrative sketch of two BWAs with opposite propagation mismatches located adjacent to each other. In Fig. 1(b) we show the propagation of a beam in the linear regime where Eq. (3) is used as input condition for numerically solving Eq. (1). Amplitudes of the beam at input (solid blue with round markers) and output (solid black) are plotted in Fig. 1(c). In Fig. 1(c) we also plot the dotted red curve representing the exact solution in the form of Eq. (4) for the discrete model represented by Eq. (1). The dotted red curve and the output solid black curve in Fig. 1(c) coincide perfectly with each other, therefore the output solid black curve is hidden behind the dotted red curve. Figure 1(d) shows the phase pattern of the beam at four propagation distances $z = 0$ (dotted red), 100 (dash-dotted blue), 150 (solid green), and 200 (dashed black). From Eqs. (3) and (4) one can easily see that as the waveguide position variable n runs, the phase pattern of the JR states must be periodic as follows: $\delta_n = \ldots(\rho,\rho),(\rho+\pi,\rho+\pi),(\rho,\rho),\ldots$, where ρ also changes with z (fields at two central waveguides $n = -1$ and 0 are in phase). These phase patterns are perfectly illustrated in Fig. 1(d). The parameters used for simulations in Fig. 1 are $-\sigma_1 = \sigma_2 = 1$, $\kappa = 1$, and $\gamma = 0$. Two BWAs consist of 841 waveguides in total.

We would like to stress that the linear JR state found above is fundamentally different from conventional defect states found in the literature [56]. The JR state, being the zero mode of the linear Dirac Hamiltonian, is much more robust than ordinary defect modes with respect to perturbations, due to its topological nature, which protects it from disorder or from distortions of the lattice. This is the whole point in using a Dirac equation rather than the conventional Schrödinger equation and therefore the use of BWAs rather than simple nonbinary WAs. We will show in the next section that the topological protection works very well also in the nonlinear state and the JR state is preserved when nonlinearity is present, making this mode of great interest for applications.

IV. LOCALIZED JACKIW-REBBI STATES IN THE NONLINEAR CASE

In Figs. 2(a) and 2(b) we show the propagation of a beam with focusing ($\gamma = 1$) and defocusing nonlinearity ($\gamma = -1$), respectively. As input condition for Figs. 2(a) and 2(b) Eq. (3) is used, but multiplied by a factor of 0.5 and 1.0 in Figs. 2(a) and 2(b), respectively. Note that the beam widths (FWHM) in Fig. 2 are larger than in Fig. 1, because in Fig. 2 we use $-\sigma_1 = \sigma_2 = 0.6$, whereas $-\sigma_1 = \sigma_2 = 1.0$ in Fig. 1 [see also Eq. (3)]. In Fig. 2(c) we plot the beam profile $|a_n|$ taken from Fig. 2(a) at four propagation distances $z = 0$ (red), 100 (blue), 200 (green), and 300 (dashed black with round markers). From Figs. 2(a) and 2(c) one can see that the input profile is slightly adjusted to a stable soliton profile, which is well conserved during propagation. As a result, the three latter curves in Fig. 2(c) are almost identical and one can clearly see only the dashed black curve with round markers, whereas two other curves (blue and green) are hidden behind this black curve. Note that for the localized state in the linear regime illustrated in Fig. 1 one has $|a_{2n-1}| = |a_{2n}|$, whereas for the established localized state in the regime with focusing nonlinearity illustrated in Figs. 2(a) and 2(c), except for the two central sites where $|a_{-1}| = |a_0|$, one has $|a_{2n-1}| < |a_{2n}|$ if $n < 0$ and $|a_{2n-1}| > |a_{2n}|$ if $n > 0$. Analogously, in Fig. 2(d) we plot the beam profile $|a_n|$ taken from Fig. 2(b) at four propagation distances $z = 0$ (red), 100 (blue), 200 (green), and 300 (dashed black with round markers). Note that in Fig. 2(d), just like in Fig. 2(c), one can also clearly see only the dashed black curve with round markers, whereas two other curves (blue and green) are hidden behind this black curve. From Figs. 2(b) and 2(d) one can see that the input profile is slightly adjusted to a stable soliton profile, which is also well conserved during propagation. Note that for the established localized state in the regime with defocusing nonlinearity illustrated in Figs. 2(b) and 2(d), except for the two central sites where $|a_{-1}| = |a_0|$, one has $|a_{2n-1}| > |a_{2n}|$ if $n < 0$ and $|a_{2n-1}| < |a_{2n}|$ if $n > 0$. It is worth mentioning that the phase patterns of two beams in Fig. 2 are also identical to the ones illustrated in Fig. 1(d). We would like to note the much greater stability of the JR state under the effect of nonlinearity with respect to conventional defect modes in WAs, which are subject to the so-called nonlinear escape (see e.g., Ref. [56]).

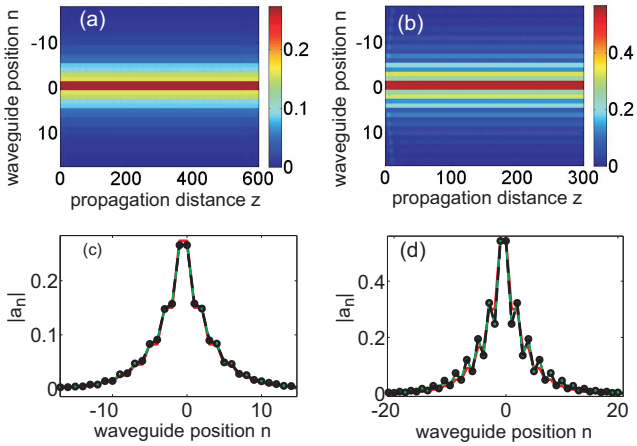

FIG. 2. Propagation of a beam with (a) focusing and (b) defocusing nonlinearity. (c) and (d) Plot of $|a_n|$ of the corresponding beam in (a) and (b), respectively, at different propagation distances $z = 0$ (red), 100 (blue), 200 (green), and 300 (dashed black with round markers). Note that the blue and green curves are hidden behind the dashed black with round markers. The parameters are $-\sigma_1 = \sigma_2 = 0.6$, $\kappa = 1$, and (a) $\gamma = 1$ and (b) $\gamma = -1$. Two BWAs consist of 841 waveguides in total. As input condition for (a) and (b) Eq. (3) is used, but multiplied by a factor of 0.5 and 1.0 in (a) and (b), respectively.

V. FORMATION OF JACKIW-REBBI STATES BY DIRAC SOLITONS

In Fig. 3(a) we show the formation of a JR state from two out-of-phase Dirac solitons. These Dirac solitons with analytical solutions are taken from Ref. [33] and are initially motionless in the transverse direction with centers at waveguides $n = \pm 10$. These two Dirac solitons repel each other during propagation and at the same time a JR state is formed at the center of the array. In Fig. 3(c) we plot the beam profiles at four propagation distances $z = 0$ (red), 100 (blue), 200 (green), and 300 (black) of the JR state shown in Fig. 3(a). In

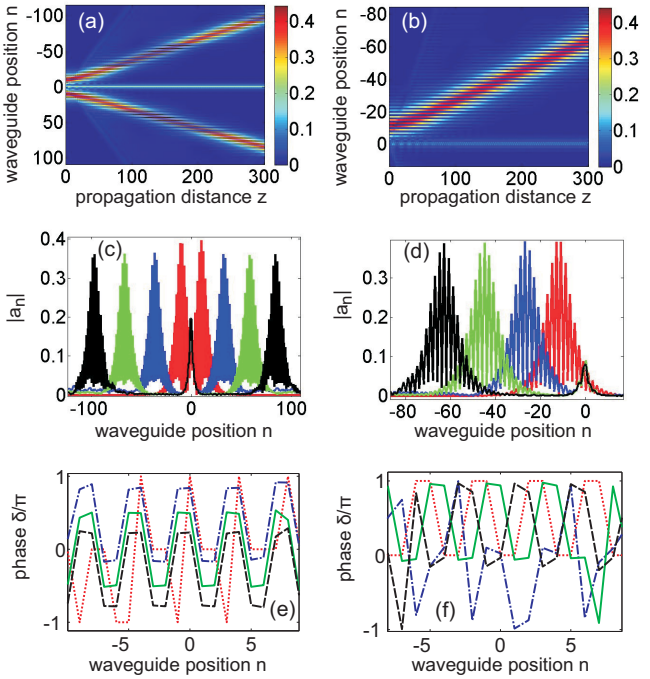

FIG. 3. (a) Formation of a JR state from two out-of-phase Dirac solitons. (b) Formation of a JR state from one Dirac soliton. (c) and (d) Plot of $|a_n|$ of the corresponding beam in (a) and (b), respectively, at different propagation distances $z = 0$ (red), 100 (blue), 200 (green), and 300 (black). (e) and (f) Phase patterns of the beams in (c) and (d), respectively at corresponding propagation distances $z = 0$ (dotted red), 100 (dash-dotted blue), 200 (solid green), and 300 (dashed black). The parameters are $\gamma = 1$, $-\sigma_1 = \sigma_2 = 1.0$, and $\kappa = 1$.

Fig. 3(e) we plot the phase patterns of the corresponding beam profiles in Fig. 3(c) at these four propagation distances $z = 0$ (dotted red), 100 (dash-dotted blue), 200 (solid green), and 300 (dashed black). It is worth emphasizing that at the input the overlapping of the two Dirac solitons is weak and we have the profile that is totally different from the one of a JR state. However, the phase pattern of the field at the center of the array at the input [see the dotted red curve in Fig. 3(e)] is identical to the one of the JR state as illustrated in Fig. 1(d) (note the trivial fact that the phase difference equal to 2π means fields are just in phase). This requirement for phase pattern at the input is crucial for formation of the JR states later during propagation. For two symmetric Dirac solitons located at two BWAs as shown in Fig. 3(a) this phase pattern is only obtained if these two Dirac solitons are initially out of phase. If this condition is satisfied, then a JR state with the right beam profile and phase pattern will be formed as clearly shown in Figs. 3(a), 3(c), and 3(e). Of course, the closer the initial Dirac solitons, the larger the amplitude of the established JR state.

We have shown in Figs. 3(a), 3(c), and 3(e) that a JR state can be formed from two out-of-phase Dirac solitons. In the same way, we show in Figs. 3(b), 3(d), and 3(f) that a quasi-JR-state can also be formed from just one Dirac soliton that is initially located close to the border of the two BWAs. However, in this case, the peak amplitude of the established quasi-JR-state as shown in Fig. 3(d) is about three times weaker than the JR state shown in Fig. 3(c). The phase pattern of this beam as illustrated in Fig. 3(f) is also not perfectly identical to the one of a true JR state.

VI. CONCLUSION

We have analytically and numerically demonstrated the existence of the optical analog of edge states, known in quantum field theory as the Jackiw-Rebbi states, formed at the interface of two BWAs having propagation mismatches with opposite signs. Remarkably, the localized JR states can be formed in both linear and nonlinear regimes and can be divided into two types with different amplitude profiles depending on the signs of propagation mismatches at the interface. We have also shown the excitation of JR states from Dirac solitons. Due to the robustness of the topological JR states, we envision important future applications in the generation of topologically protected correlated photons, using a similar scheme as proposed recently in Ref. [51].

ACKNOWLEDGMENT

This research is funded by Vietnam National Foundation for Science and Technology Development (NAFOSTED) under Grant No. 103.03-2016.01.

[1] D. N. Christodoulides, F. Lederer, and Y. Silberberg, Nature (London) **424**, 817 (2003).
[2] A. L. Jones, J. Opt. Soc. Am. **55**, 261 (1965).
[3] D. N. Christodoulides and R. I. Joseph, Opt. Lett. **13**, 794 (1988).
[4] K. G. Makris, J. Hudock, D. N. Christodoulides, G. I. Stegeman, O. Manela, and M. Segev, Opt. Lett. **31**, 2774 (2006).
[5] S. Suntsov, K. G. Makris, D. N. Christodoulides, G. I. Stegeman, R. Morandotti, M. Volatier, V. Aimez, R. Arès, C. E. Rüter, and D. Kip, Opt. Express **15**, 4663 (2007).
[6] S. Suntsov, K. G. Makris, D. N. Christodoulides, G. I. Stegeman, R. Morandotti, M. Volatier, V. Aimez, R. Arès, E. H. Yang, and G. Salamo, Opt. Express **16**, 10480 (2008).
[7] Y. V. Kartashov, V. A. Vysloukh, and L. Torner, Phys. Rev. Lett. **96**, 073901 (2006).
[8] Y. Kominis, A. Papadopoulos, and K. Hizanidis, Opt. Express **15**, 10041 (2007).
[9] Y. Kominis and K. Hizanidis, Phys. Rev. Lett. **102**, 133903 (2009).
[10] S. Suntsov, K. G. Makris, D. N. Christodoulides, G. I. Stegeman, A. Haché, R. Morandotti, H. Yang, G. Salamo, and M. Sorel, Phys. Rev. Lett. **96**, 063901 (2006).
[11] C. R. Rosberg, D. N. Neshev, W. Krolikowski, A. Mitchell, R. A. Vicencio, M. I. Molina, and Y. S. Kivshar, Phys. Rev. Lett. **97**, 083901 (2006).
[12] E. Smirnov, M. Stepić, C. E. Rüter, D. Kip, and V. Shandarov, Opt. Lett. **31**, 2338 (2006).
[13] F. Lederer, G. I. Stegeman, D. N. Christodoulides, G. Assanto, M. Segev, and Y. Silberberg, Phys. Rep. **463**, 1 (2008).
[14] T. Pertsch, P. Dannberg, W. Elflein, A. Bräuer, and F. Lederer, Phys. Rev. Lett. **83**, 4752 (1999).
[15] R. Morandotti, U. Peschel, J. S. Aitchison, H. S. Eisenberg, and Y. Silberberg, Phys. Rev. Lett. **83**, 4756 (1999).

[16] M. Ghulinyan, C. J. Oton, Z. Gaburro, L. Pavesi, C. Toninelli, and D. S. Wiersma, Phys. Rev. Lett. **94**, 127401 (2005).
[17] H. Trompeter, T. Pertsch, F. Lederer, D. Michaelis, U. Streppel, A. Bräuer, and U. Peschel, Phys. Rev. Lett. **96**, 023901 (2006).
[18] T. X. Tran and F. Biancalana, Phys. Rev. Lett. **110**, 113903 (2013).
[19] T. X. Tran and F. Biancalana, Opt. Exp. **21**, 17539 (2013).
[20] T. X. Tran, D. C. Duong, and F. Biancalana, Phys. Rev. A **89**, 013826 (2014).
[21] S. Longhi, Phys. Rev. B **81**, 075102 (2010).
[22] F. Dreisow, R. Keil, A. Tünnermann, S. Nolte, S. Longhi, and A. Szameit, Europhys. Lett. **97**, 10008 (2012).
[23] S. Longhi, Opt. Lett. **35**, 235 (2010).
[24] F. Dreisow, M. Heinrich, R. Keil, A. Tünnermann, S. Nolte, S. Longhi, and A. Szameit, Phys. Rev. Lett. **105**, 143902 (2010).
[25] S. Longhi, Appl. Phys. B **104**, 453 (2011).
[26] J. M. Zeuner, N. K. Efremidis, R. Keil, F. Dreisow, D. N. Christodoulides, A. Tünnermann, S. Nolte, and A. Szameit, Phys. Rev. Lett. **109**, 023602 (2012).
[27] A. A. Sukhorukov and Y. S. Kivshar, Opt. Lett. **27**, 2112 (2002).
[28] M. Conforti, C. De Angelis, and T. R. Akylas, Phys. Rev. A **83**, 043822 (2011).
[29] R. Morandotti, D. Mandelik, Y. Silberberg, J. S. Aitchison, M. Sorel, D. N. Christodoulides, A. A. Sukhorukov, and Y. S. Kivshar, Opt. Lett. **29**, 2890 (2004).
[30] M. Johansson, K. Kirr, A. S. Kovalev, and L. Kroon, Phys. Scr. **83**, 065005 (2011).
[31] A. Gorbach and M. Johansson, Eur. Phys. J. D **29**, 77 (2004).
[32] Y. S. Kivshar and N. Flytzanis, Phys. Rev. A **46**, 7972 (1992).
[33] T. X. Tran, S. Longhi, and F. Biancalana, Ann. Phys. (NY) **340**, 179 (2014).
[34] T. X. Tran, X. N. Nguyen, and D. C. Duong, J. Opt. Soc. Am. B **31**, 1132 (2014).
[35] T. X. Tran, X. N. Nguyen, and F. Biancalana, Phys. Rev. A **91**, 023814 (2015).
[36] T. X. Tran and D. C. Duong, Ann. Phys. (NY) **361**, 501 (2015).
[37] A. Marini, S. Longhi, and F. Biancalana, Phys. Rev. Lett. **113**, 150401 (2014).
[38] N. J. Poplawski, Phys. Rev. D **85**, 107502 (2012).
[39] W. Heisenberg, Rev. Mod. Phys. **29**, 269 (1957).
[40] D. C. Ionescu, J. Reinhardt, B. Muller, W. Greiner, and G. Soff, Phys. Rev. A **38**, 616 (1988).
[41] A. Zecca, Int. J. Theor. Phys. **41**, 421 (2002).
[42] M. J. Esteban and E. Séré, Discrete Cont. Dyn. Syst. **8**, 381 (2002).
[43] I. Bialynicki-Birula and J. Mycielski, Ann. Phys. (NY) **100**, 62 (1976).
[44] L. Lu, J. D. Joannopoulos, and M. Soljačic, Nat. Photon. **8**, 821 (2014).
[45] M. C. Rechtsman, J. M. Zeuner, Y. Plotnik, Y. Lumer, D. Podolsky, F. Dreisow, S. Nolte, M. Segev, and A. Szameit, Nature (London) **496**, 196 (2013).
[46] R. Jackiw and C. Rebbi, Phys. Rev. D **13**, 3398 (1976).
[47] R. B. Laughlin, Rev. Mod. Phys. **71**, 863 (1999).
[48] M. Z. Hasan and C. L. Kane, Rev. Mod. Phys. **82**, 3045 (2010).
[49] X. L. Qi and S. C. Zhang, Rev. Mod. Phys. **83**, 1057 (2011).
[50] N. Malkova, I. Hromada, X. Wang, G. Bryant, and Z. Chen, Opt. Lett. **34**, 1633 (2009).
[51] A. Blanco-Redondo, I. Andonegui, M. J. Collins, G. Harari, Y. Lumer, M. C. Rechtsman, B. J. Eggleton, and M. Segev, Phys. Rev. Lett. **116**, 163901 (2016).
[52] J. Ruostekoski, G. V. Dunne, and J. Javanainen, Phys. Rev. Lett. **88**, 180401 (2002).
[53] T. Yefsah, A. T. Sommer, M. J. H. Ku, L. W. Cheuk, W. Ji, W. S. Bakr, and M. W. Zwierlein, Nature (London) **499**, 426 (2013).
[54] D. G. Angelakis, P. Das, and C. Noh, Sci. Rep. **4**, 6110 (2014).
[55] R. Keil, C. Noh, A. Rai, S. Stützer, S. Nolte, D. G. Angelakis, and A. Szameit, Optica **2**, 454 (2015).
[56] U. Peschel, R. Morandotti, J. S. Aitchison, H. S. Eisenberg, and Y. Silberberg, Appl. Phys. Lett. **75**, 1348 (1999).